



Research paper

Precise microsampling of poorly laminated speleothems for U-series dating

Russell N. Drysdale^{a,*}, Bence T. Paul^b, John C. Hellstrom^b, Isabelle Couchoud^{a,c}, Alan Greig^b, Petra Bajo^a, Gianni Zanchetta^{d,e,f}, Ilaria Isola^f, Christoph Spötl^g, Ilaria Baneschi^e, Eleonora Regattieri^d, Jon D. Woodhead^b

^a Department of Resource Management and Geography, University of Melbourne, 221 Bouverie St., Parkville 3010, Victoria, Australia

^b School of Earth Sciences, University of Melbourne, Parkville 3010, Victoria, Australia

^c Laboratoire EDYTEM, UMR 5204, Université de Savoie, 73376 Le Bourget du Lac cedex, France

^d Department of Earth Sciences, University of Pisa, Pisa 56100, Italy

^e Istituto di Georisorse e Geoscienza-CNR, Pisa 56100, Italy

^f Istituto Nazionale di Geofisica e Vulcanologia, Pisa 56100, Italy

^g Institut für Geologie und Paläontologie, Universität Innsbruck, Innrain 52, 6020 Innsbruck, Austria

ARTICLE INFO

Article history:

Received 5 January 2012

Received in revised form

26 June 2012

Accepted 29 June 2012

Available online 11 July 2012

Keywords:

Speleothems

U–Th dating

Growth layers

LA-ICP-MS

Trace elements

Microsampling

ABSTRACT

One of the principal reasons why speleothems are recognised as important palaeoclimate archives is their suitability for accurate and precise uranium-series (U-series) age determination. Sampling speleothem sections for U-series dating is straightforward in most cases because visible growth layers are preserved. However, this is not always the case, and here we describe a sampling strategy whereby growth layers are resolved from trace-element images produced by laser-ablation inductively coupled plasma mass spectrometry (LA-ICP-MS). We apply this method to a section of an Italian subaqueous speleothem (CD3) that lacks persistent visible growth layering.

Trace-element imaging revealed growth layers that are strongly non-planar in their geometry owing to the speleothem's pronounced euhedral crystal terminations. The most prominent trace-element layers were first digitized as x, y vector contours. We then interpolated these in the growth-axis direction to generate a series of contour lines at $\sim 250\text{-}\mu\text{m}$ increments. The coordinates of these contours were used to guide the sampling via a computerised micromilling lathe. This produced a total of 22 samples for U-series dating by multi-collector ICP-MS. The dating results returned ages in correct stratigraphic order within error. Close inspection of the U-series data and the derived depth–age model suggests that the main source of model-age uncertainty is unrelated to the contour sampling but instead more associated with how closely spaced the model ages are in time, i.e. the model age density. Comparisons between stable oxygen and carbon isotope profiles derived from aliquots of the dating samples and two other stable isotope profiles from CD3 spanning the same time period compare very favourably. Taken together, this suggests that our trace-element contouring method provides a reliable means for extracting samples for dating (and other geochemical analyses), and can be applied to similar speleothems lacking visible growth layering.

© 2012 Elsevier B.V. All rights reserved.

1. Introduction

In common with marine and lake sediments and polar ice cores, speleothems possess a relatively large number of physical and chemical properties that can be used as proxies for past climate and environmental change (Fairchild et al., 2006). One of their key features, however, is their suitability for accurate and precise age determination by uranium-series (U-series) methods (Richards and

Dorale, 2003). An important precursor to developing a reliable and robust U-series chronology is the integrity of the sampling for dating once the speleothem has been collected. The investigator must resolve the sampling positions for dating as precisely as possible to minimise sampling uncertainty, which in turn will improve both the precision and accuracy of the depth–age relationship to which the palaeoclimate proxy data of the speleothem are anchored.

Sampling uncertainty for stalagmites, the most common form of speleothem used in palaeoclimate research, can easily be minimised because they usually possess visible layering and they

* Corresponding author. Tel.: +61 3 8344 9318.

E-mail address: rnd@unimelb.edu.au (R.N. Drysdale).

accumulate at a sufficiently fast rate that the practical task of extracting datable material is quite straightforward. Compared with other speleothem types, stalagmites offer the best prospects for assembling highly resolved, well-dated palaeoclimate time series. Yet relatively few stalagmites reported in the literature show evidence for continuous growth in excess of several tens of thousands of years because they are usually deposited from single drip points that, for a multitude of reasons, are susceptible to flow interruptions and shifts in the position of the discharge point. Such interruptions limit the range of palaeoclimate problems to which stalagmites can be applied.

To assemble continuous palaeoclimate records over longer time intervals it may be necessary to target speleothem types that are less likely to experience growth interruptions. Flowstones potentially meet this criterion. They are often fed by multiple point sources and are thus more likely to experience long periods of continuous growth. Yet flowstones have several problems that render them much more difficult to sample than stalagmites. For example, the presence of microgours and other surface micro-scale relief features can create a layer architecture that is three-dimensionally complex. In addition, water movement across a flowstone is affected by the surface micromorphic evolution, resulting in synchronous areas of deposition and non-deposition. This can lead to misinterpretation of growth hiatuses and to inflated or deflated rates of growth, which can complicate the age sampling procedure.

Speleothems formed in supersaturated subaqueous environments, such as cave pools in the vadose zone or phreatic galleries where there is an atmosphere into which degassing can take place, offer better prospects for long and continuous records. Although not formed in a karst cave, the Devil's Hole vein calcite is a splendid example of a subaqueous speleothem yielding a long and continuous palaeoclimate record: it preserves a precisely dated time series of changes in the stable oxygen ($\delta^{18}\text{O}$) and carbon ($\delta^{13}\text{C}$) isotope composition of regional groundwaters spanning almost 560 kyr (Winograd et al., 1992; Winograd, 2002; Coplen et al., 1994). However, as in the case of flowstones, subaqueous deposits also have shortcomings with regards to sampling. For example, the calcite of which they are usually comprised often possesses euhedral crystal terminations, which by their very nature do not produce the planar or sub-planar laminations that so usefully guide the sampling of many stalagmites and flowstones. In addition, typical growth rates of subaqueously-deposited calcite are at the low end of rates found in speleothems thus limiting their applicability to resolve proxy changes at high temporal resolution. Nevertheless, given their high potential for long and continuous growth, such deposits have much to offer palaeoclimate research and therefore warrant investigation as to the ways in which this growth layer problem might be resolved.

We present details of a precise microsampling method applied to a subaqueous speleothem (CD3) that not only possesses non-planar growth layering but also contains sections lacking any form of visible layering. The method is potentially applicable to all speleothems that have poorly resolved or unresolved growth layers. It uses contouring information derived from two-dimensional trace-element maps produced by laser-ablation inductively coupled plasma mass spectrometry (LA-ICP-MS) (Woodhead et al., 2007). We evaluate our method by investigating the sources of uncertainty in the U-series ages and by comparing stable isotope profiles developed from aliquots of these dating samples with existing isotope profiles of CD3.

2. Sample location and description

The sample used in this study (CD3) was collected from a small pool ('Laghetto Basso') in Corchia Cave, Italy. The pool

has developed on the floor of the 'Galleria delle Stalattiti', a chamber situated about 800 m from the nearest entrance of the cave (Piccini et al., 2008). The pool has a maximum depth of ~0.5 m and trends parallel to the strike of a set of steeply dipping dolomitic marble and marble beds. It is fed by drips falling from a long row of stalactite curtains that have grown from percolation waters issuing through fractures in these beds, and drains at its northern extremity via a narrow sill. *In situ* temperature and pH measurements and elemental and isotopic analyses of water samples collected over a 10-year period (Baneschi et al., 2011) show that the pool waters are physically and chemically stable. This suggests the waters are significantly mixed by the time they traverse the >400 m of rock *en route* to the chamber.

The entire perimeter of Laghetto Basso is coated with a subaqueous carbonate crust similar to the "mammillary calcite" found in the Devils Hole system (e.g. Winograd et al., 1992; Kolesar and Riggs, 1999, 2004). The morphology of the crust displays numerous gently domed mounds and protuberances, the incidence of which is related to the relief of the bedrock substrate as well as the presence of broken stalactites on the pool floor. CD3 is a core recovered from one of the more prominent subaqueous mounds using a battery-powered drill fitted with a diamond-crowned core barrel (Spötl and Matthey, 2012). It measures only ~260 mm in length (Fig. 1a), and is composed entirely of calcite except for a few thin (~0.2–2 mm) layers comprising admixtures of calcite and aragonite that occur towards the base. The crystalline fabric of this mammillary calcite resembles the palisade calcite of Folk and Assereto (1976), with large columnar crystals (up to 3 mm wide and 30 mm long) oriented mostly perpendicular to the growth surface and with virtually no inter-crystalline porosity. In thin section, each columnar crystal displays an undulatory extinction in its central part and a plumose texture towards its edges. The coarse pale-yellow to light-brown banding observable in polished section (Fig. 1a) is due to changes in the abundance of micro-inclusions. Preliminary organic fluorescence analysis suggests that these inclusions are at least partly organic in origin (Drysdale et al., 2011).

Reconnaissance dating by $^{230}\text{Th}/^{234}\text{U}/^{238}\text{U}$ methods reveals that the stable-isotope, organic-fluorescence and trace-element geochemistry profiles of CD3 preserve an apparently continuous palaeoclimate record spanning almost the last million years (Drysdale et al., 2011). The deposit thus has an exceptionally slow growth rate (~0.3 mm kyr⁻¹). Its actively growing surface is highly irregular due to the euhedral to subhedral terminations of the calcite crystals (Fig. 1b). This irregularity is apparent throughout the core in places where layering visible to the naked eye occurs. However, large sections of the core lack visible laminations. Together with the euhedral crystal form and slow growth rate, this makes it extremely challenging to recover precisely located dating samples at a satisfactory spatial resolution. Reconnaissance ages on the core obtained from plunge drilling have allowed us to produce a very rudimentary age model but the ages obtained from sections lacking visible laminations impose large sampling uncertainties. We considered using laser-ablation U-series dating, which has been shown to produce meaningful results on samples containing U concentrations similar to those in CD3 (~1.0 ± 0.5 ppm) (Eggins et al., 2005). This method was deemed inappropriate, however, given the level of precision required for our work (i.e. 2σ uncertainties <5% of the calculated age). Consequently, we sought to reduce the level of uncertainty by developing a new sampling method based on trace element mapping. To illustrate this method, we focus on a section of CD3 that captures the period ~300–220 ka (Fig. 1c), which includes the Marine Isotope Stage 8–7 glacial-to-interglacial transition.

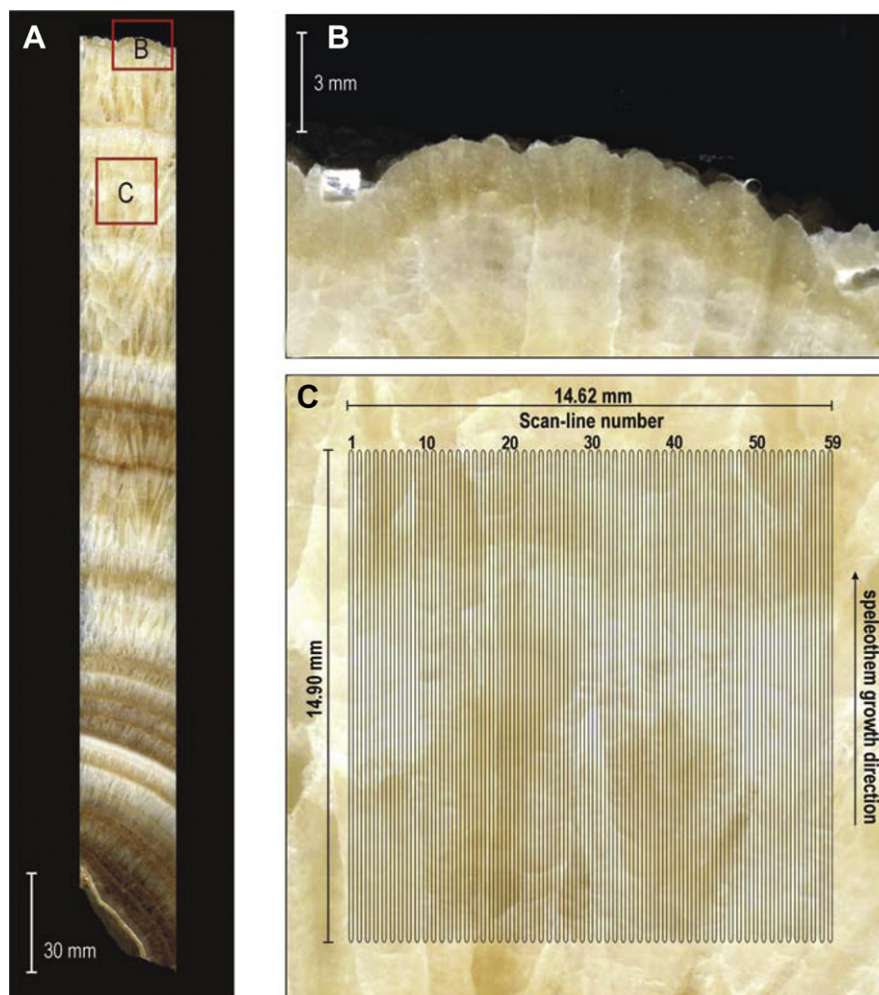


Fig. 1. (A) Polished section of the Laghetto core. (B) Detail of the core-top surface showing non-planar, euhedral to subhedral crystal terminations. (C) The section studied in this paper, showing general absence of laminations. The grid of laser ablation scan lines (drawn to scale) is also shown. In this view, the x-axis (as referred to in the text and in Figs. 3 and 4) runs vertically.

3. Methods

3.1. Trace element mapping

The approximate position in CD3 of the time interval of interest was identified by pattern-matching its $\delta^{18}\text{O}$ and $\delta^{13}\text{C}$ profiles with that of a U-series dated stalagmite from the same cave (Couchoud et al., 2011) and the deep-sea benthic $\delta^{18}\text{O}$ and sea-surface temperature record from the Iberian margin (Martrat et al., 2007). The trace-element analyses were performed on a section measuring 14.90 mm \times 14.62 mm (Fig. 1c) using a 193 nm ArF-excimer laser-ablation system coupled to an Agilent 7700x quadrupole ICP-MS. The operating conditions of the laser and ICP-MS, as well as the elements/masses that were analysed, are summarised in Table 1. After 2×15 min steps of ultra-sonication in double-deionised water, the sample was fitted into the sample holder of the laser system, which moves in x, y via a computerised stage. The Helex laser ablation system, which has been described previously (e.g. Woodhead et al., 2007), is driven using the GeoStar software produced by Resonetics, and was set up to ablate the section in 59 parallel tracks, the centres of which were spaced 250 μm apart. Each track was twice pre-ablated using a 200- μm circular spot at a scan speed of 20 mm min^{-1} and a laser pulse rate of 15 Hz. The trace element data were then derived from the pre-ablated surface

using a 120- μm circular spot at a scan rate of 6 mm min^{-1} and a laser pulse rate of 10 Hz. Ablation took place in an environment of ultra-high-purity helium with the ablated aerosol then carried in an ultra-high-purity argon stream into the mass spectrometer.

Table 1
Instrumental operating conditions for the LA-ICP-MS.

<i>Agilent 7700x ICP-MS</i>	
Forward power	1300 W
Reflected power	2 W
Sample depth	3 mm
Dwell time	0.01 s
Carrier gas	0.89 l min^{-1}
<i>Helex laser ablation system</i>	
Lambda Physik Compex 110 ArF excimer	193 nm
Laser fluence	$\sim 5 \text{ J cm}^{-2}$
Pre-ablation spot size	200 μm
Data collection spot size	120 μm
Pre-ablation repetition rate	15 Hz
Data collection repetition rate	10 Hz
He gas to cell	500 ml min^{-1}
Masses measured (m/z)	25Mg, 43Ca, 88Sr, 138Ba, 232Th, 238U

Elemental concentrations were calibrated against the NIST SRM612 glass reference with the isotope ^{43}Ca used as an internal standard to monitor and correct for instrument drift. Given our focus on producing maps highlighting *relative*, rather than *absolute*, changes in trace element concentrations, additional reference standards were not used for calibration. Raw mass spectrometry data were reduced using the software Iolite (Hellstrom et al., 2008; Paton et al., 2011) using the image creation technique described in Paul et al. (2012). A laser log file was produced by the GeoStar software, which records the laser state, the position of the laser spot, and the laser spot size against a timestamp. This log file was imported into Iolite, and interpolated to the same sampling density as the mass spectrometry data. Using the laser position and mass spectrometry data, we were able to plot the composition at each sampling location. Due to laser spot overlap, some pixels in the image may have two or more mass spectrometer readings. Where this was the case, the mean of the measurements was used (see Paul et al. (2012) for more detail). Values were then linearly interpolated between scan lines, and plots for Mg, Sr, Ba, U and Th were saved as images (Fig. 2a–e).

Previous LA-ICP-MS analyses on CD3 revealed the following rank-order characteristics in terms of reproducible trace elements patterns with laterally consistent concentrations: magnesium (Mg) \gg strontium (Sr) = barium (Ba) \gg uranium (U) $>$ thorium (Th). This general pattern is evident in Fig. 2a–e, with Mg, Sr and Ba having by far the best-defined chemical laminae. Accordingly, these elements were used to develop trace element maps for this study. The U map shows evidence for considerable concentration heterogeneity within the section. This distribution appears to be

strongly related to crystal orientation rather than leaching, given the fan-shaped nature of the darker (i.e. lower-concentration) U zones (Fig. 2d) and the higher-concentration zoning shown in the corresponding regions of the Sr (Fig. 2b) and Ba (Fig. 2c) maps. The Th map (Fig. 2e) shows no evidence of Th-rich laminae that could affect the quality of the U-series ages.

3.2. Data processing

The processed trace-element images were imported into the program *Digitizelt* (Bormissoft, Germany), which generated x , y coordinates of vector-line contours produced by on-screen digitisation of individual trace-element layers. For each image, the top-left and bottom-right margins of the image were identified and referenced using the coordinates from the laser-ablation sample-stage software. Individual contour lines in an image were digitised by eye via the computer mouse. Only the most obvious contours that could be traced continuously across each image were used (Fig. 3a).

The complete sequence of manually digitised contour coordinates was imported into a spreadsheet in preparation for interpolation. The nominal down-axis increment for the subsequent micromilling was $250\ \mu\text{m}$. However, because the manually digitised contours were spaced at intervals greater than $250\ \mu\text{m}$ (Fig. 3a), interpolation between successive contour pairs was necessary. This was achieved by first interpolating *across* each contour at $100\text{-}\mu\text{m}$ increments (i.e. for each digitised contour line, a string of x , y coordinates was generated at intervals of $x = 100\ \mu\text{m}$). Second, interpolation *between* each successive pair of contours was

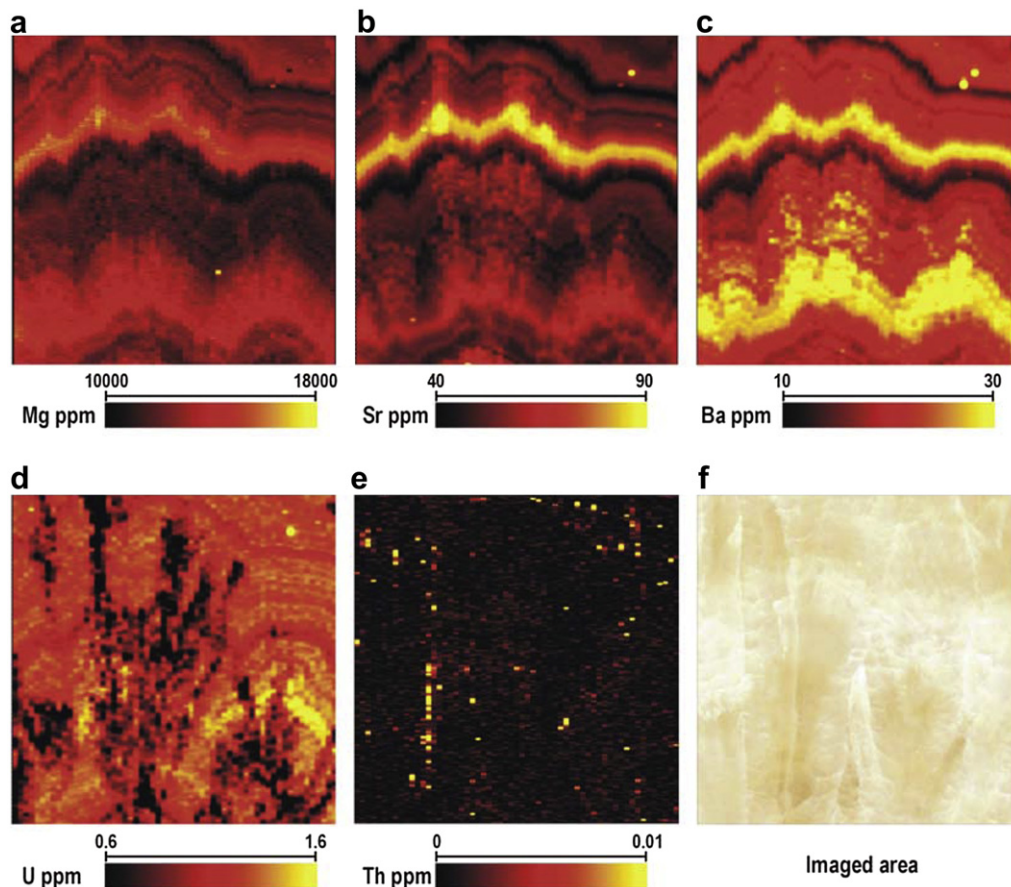


Fig. 2. (a) Mg, (b) Sr, (c) Ba, (d) U and (e) Th element maps for the laser-scanned section (f). Grid dimensions are shown in Fig. 1.

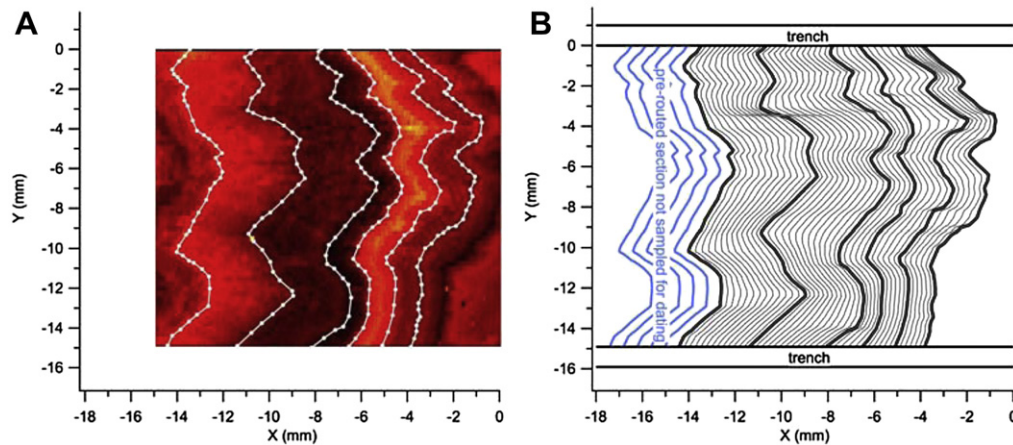


Fig. 3. (A) The raw data points (white bullets) of the composite set of manually digitised points from the trace element maps superimposed over the Mg map. The white lines are the contours derived from interpolating the raw data points at 100- μm intervals in the y direction. (B) Grey lines are the full suite of 43 contours milled for the U-series age dating. The heavy grey lines are the contours interpolated from the manual digitising (i.e. the white lines in (A)); the thinner grey lines are the contours interpolated between these – see text for explanation. The blue contours were pre-routed below the sampled section to facilitate powder collection. The position of two trenches, which were routed to prevent contamination at the end of each sweep of the milling bit, are also shown. (For interpretation of the references to colour in this figure legend, the reader is referred to the web version of this article.)

conducted in the x (growth-axis) direction using an interval as close as possible to $y = 250 \mu\text{m}$. The number of interpolated contours per manually digitised contour pair was calculated by dividing the mean distance between these pairs by $250 \mu\text{m}$; rounding up or down to obtain a whole number of interpolated contours resulted in a mean layer thickness over the whole section varying between 231 and $265 \mu\text{m}$ (Fig. 3b). This variation is reflected in the spacing between successive depth centres shown in Table 2.

3.3. Micromilling

A TAIG CNC micromilling lathe was used to micromill the dating samples. To achieve this, the coordinate information from both the

manually digitised and the interpolated contours was converted to the G-code format utilised by the lathe's software, *MPS2003*. In this format, each line of code represents a direction + distance command. To set up the milling, the sample block was clamped to the micromill stage then carefully aligned using four control points that were laser-drilled into the block whilst it was inside the laser sample holder. Milling was performed using a 0.8 mm end-mill bit, which was driven by the milling software across the sample at the range of sample-thickness increments dictated by the contouring, as described above. Sampling commenced at the stratigraphically oldest end of the speleothem section. To facilitate the collection of the first few sample powders, a $\sim 4 \text{ mm}$ -long section was routed out by interpolating the oldest contour 'back in time' in a series of

Table 2

Measured U and Th isotope activity ratios and derived corrected ages and initial U isotope ratios for the studied section of CD3.

Sample code	Sample depth ^a mm (\pm)	U (ppb)	$(^{230}\text{Th}/^{238}\text{U})^b$ (2σ)	$(^{234}\text{U}/^{238}\text{U})$ (2σ)	$(^{232}\text{Th}/^{238}\text{U}) \times 1000$ (2σ)	Age ka corrected ^c (2σ)	$(^{234}\text{U}/^{238}\text{U})_i$ corrected ^d (2σ)	$(^{230}\text{Th}/^{232}\text{Th})$	
CD3-227	0.12 (0.32)	993	0.6835 (0.0027)	0.8250 (0.0012)	0.1028 (0.0106)	229.0 (5.0)	0.6659	0.0073	6650
CD3-227	0.12 (0.32)	993	0.6835 (0.0027)	0.8250 (0.0012)	0.1028 (0.0106)	229.0 (5.0)	0.6659	0.0073	6650
CD3-226	0.58 (0.63)	1284	0.6861 (0.0015)	0.8262 (0.0007)	0.0896 (0.0014)	230.6 (3.9)	0.6667	0.0061	7660
CD3-225	1.04 (0.63)	1278	0.6927 (0.0013)	0.8281 (0.0009)	0.0932 (0.0013)	236.9 (4.1)	0.6643	0.0066	7430
CD3-224	1.54 (0.65)	1372	0.6932 (0.0021)	0.8304 (0.0007)	0.1086 (0.0010)	234.0 (4.5)	0.6715	0.0064	6380
CD3-223	2.07 (0.66)	1396	0.6980 (0.0026)	0.8305 (0.0014)	0.0621 (0.0043)	240.8 (5.7)	0.6653	0.0083	11,200
CD3-222	2.60 (0.66)	1530	0.6969 (0.0016)	0.8306 (0.0008)	0.1021 (0.0006)	238.8 (4.4)	0.6675	0.0066	6820
CD3-221	3.11 (0.65)	1397	0.7017 (0.0025)	0.8325 (0.0006)	0.0747 (0.0007)	243.0 (5.3)	0.6672	0.0071	9400
CD3-220	3.60 (0.64)	1184	0.7079 (0.0019)	0.8327 (0.0008)	0.1774 (0.0106)	252.4 (5.4)	0.6586	0.0077	3990
CD3-219	4.08 (0.64)	1088	0.7134 (0.0021)	0.8374 (0.0009)	0.1596 (0.0009)	252.4 (5.5)	0.6683	0.0078	4470
CD3-218	4.59 (0.65)	1236	0.7277 (0.0025)	0.8423 (0.0014)	0.1864 (0.0017)	267.7 (7.5)	0.6640	0.0104	3900
CD3-217	5.10 (0.65)	1635	0.7290 (0.0021)	0.8422 (0.0011)	0.1455 (0.0016)	270.4 (6.8)	0.6613	0.0095	5010
CD3-216	5.61 (0.65)	1367	0.7306 (0.0034)	0.8441 (0.0014)	0.1193 (0.0020)	269.4 (8.7)	0.6662	0.0112	6120
CD3-215	6.12 (0.65)	1127	0.7380 (0.0017)	0.8456 (0.0006)	0.2099 (0.0011)	281.0 (6.8)	0.6582	0.0091	3520
CD3-214	6.63 (0.65)	1124	0.7389 (0.0024)	0.8467 (0.0010)	0.2591 (0.0021)	280.1 (7.7)	0.6615	0.0101	2850
CD3-213	7.13 (0.65)	1125	0.7423 (0.0017)	0.8496 (0.0010)	0.2048 (0.0014)	280.0 (7.0)	0.6679	0.0096	3630
CD3-212	7.64 (0.65)	1200	0.7464 (0.0016)	0.8506 (0.0008)	0.1812 (0.0007)	286.4 (7.1)	0.6640	0.0097	4120
CD3-211	8.15 (0.65)	1352	0.7453 (0.0015)	0.8508 (0.0010)	0.5734 (0.0022)	283.0 (7.0)	0.6678	0.0097	1300
CD3-210	8.65 (0.65)	1176	0.7471 (0.0015)	0.8525 (0.0011)	0.1537 (0.0011)	282.7 (7.1)	0.6719	0.0098	4860
CD3-209	9.16 (0.65)	1242	0.7494 (0.0012)	0.8520 (0.0008)	0.1029 (0.0074)	289.4 (7.0)	0.6644	0.0097	7280
CD3-208	9.66 (0.65)	1109	0.7487 (0.0018)	0.8511 (0.0009)	0.0439 (0.0009)	290.0 (7.9)	0.6619	0.0105	17,060
CD3-207	10.17 (0.65)	1226	0.7505 (0.0015)	0.8527 (0.0012)	0.0636 (0.0008)	289.7 (7.7)	0.6658	0.0108	11,800
CD3-206	10.68 (0.65)	1199	0.7530 (0.0015)	0.8530 (0.0009)	0.1146 (0.0012)	295.0 (7.9)	0.6613	0.0106	6570

^a 'Sample depth' is the relative stratigraphic position of the centre of each milled sample; the (\pm) value is the maximum stratigraphic thickness of the sample either side of this central position, and is based on a conservative estimate of sampling errors and milling bit diameter – see text for detailed explanation.

^b Brackets indicate activities.

^c Ages were corrected using an initial ($^{230}\text{Th}/^{232}\text{Th}$) activity of 1.5 ± 1.5 (2σ) and applying the decay constants of Cheng et al. (2000).

^d Calculated from the corrected ages and age uncertainties in the two previous columns.

0.8–0.6 mm steps (Fig. 3b). This produced a step-like face, from which the sample material was removed by the milling bit in much the same way as the removal of coal from an open-cut section. About 13–15 mg of powders was produced from each ca. 250 μm pass of the milling bit.

To limit sampling uncertainty in the sample depth (z) dimension, which is unavoidable due to a lack of visible information on the growth-layer trajectory ‘through the speleothem’, the milling depth was set to 0.8 mm (see below). To eliminate contamination by calcite milled just beyond the x, y limits of each contour line traverse, a pair of trenches was routed along the margins of the target area (Fig. 3b). An extra line of G-code was also written for each contour line to drive the milling bit beyond the final coordinate point of each contour and into the trench (Fig. 3b).

Finally, to eliminate cross-contamination of the powders the sample surface and milling bit were cleaned with compressed air (discharged into a vacuum exhaust system) then thoroughly cleaned in ethanol. Although recovery of solid samples is more ideal, the need to keep sample thickness to a minimum given the slow growth rate compelled us to mill powdered samples.

3.4. Isotopic dating and age-model

Uranium–thorium dating was performed on a Nu Instruments multi-collector inductively coupled mass spectrometer (MC-ICP-MS) largely following the method of Hellstrom (2003). Briefly, samples were dissolved and a mixed ^{236}U – ^{233}U – ^{229}Th spike was added prior to removal of the carbonate matrix with ion-exchange resin. The purified U and Th fraction was introduced in a dilute nitric acid to the MC-ICP-MS. The $^{230}\text{Th}/^{238}\text{U}$ and $^{234}\text{U}/^{238}\text{U}$ activity ratios were calculated from the measured atomic ratios using an internally standardised parallel ion-counter procedure and calibrated against the secular equilibrium standard, HU-1. This differed slightly from Hellstrom (2003) in that calibration of the high-mass ion counter was achieved using $^{233}\text{U}/^{236}\text{U}$ rather than $^{235}\text{U}/^{238}\text{U}$, allowing ^{238}U beams of greater than ~ 5 V intensity to be accommodated. A correction for an initial $^{230}\text{Th}/^{232}\text{Th}$ activity of 1.5 ± 1.5 was applied based on our previous age measurements of Corchia speleothems.

A Monte Carlo-based procedure was used to develop an age model and age uncertainty time series from the U-series results, and is based on a routine previously described in Drysdale et al. (2005) and modified according Hendy et al. (2012) and Scholz et al. (2012). Uncertainties from the U-series measurements as well as those from the sampling procedure are fully propagated into the output from the modelling.

3.5. Stable isotope analyses

An aliquot of ~ 1.5 mg was sub-sampled from each of the dating samples for $\delta^{18}\text{O}$ and $\delta^{13}\text{C}$ analyses. The analyses were conducted using continuous-flow isotope ratio mass spectrometry (CF-IRMS) following the method previously described in Drysdale et al. (2009) and employing an AP2003 instrument at the Department of Resource Management and Geography at the University of Melbourne. Sample results were normalised to the V-PDB scale using a Carrara Marble standard (NEW1) previously calibrated using the international standards NBS-18 and NBS-19. Analytical uncertainty for $\delta^{18}\text{O}$ and $\delta^{13}\text{C}$ were 0.09% and 0.05% respectively.

The stable isotope results from the dating-sample series were compared with data from two previous sets of $\delta^{18}\text{O}$ and $\delta^{13}\text{C}$ analyses spanning the same interval of CD3 (Drysdale et al. in preparation). These profiles were developed from within a few centimetres of the dating samples. The first comprises a continuous 1 mm series produced by plunge drilling using a 1 mm diameter

drill bit to a depth of 2 mm and employing the same model TAIG CNC micromill as that used for the age sampling. This reconnaissance series was drilled and analysed in 2007 to provide a ‘first-pass’ indication of the isotopic composition of CD3. The powders were analysed using a GV2003 CF-IRMS housed at the University of Newcastle (Australia) using exactly the same method as described above. The analytical uncertainty for $\delta^{18}\text{O}$ and $\delta^{13}\text{C}$ during these analyses based on the analysis of 70 NEW1 standards were 0.08% and 0.06% respectively.

The second series was sampled at 200- μm resolution using a New Wave Research Micromill and analysed by CF-IRMS at the Institut für Geologie und Paläontologie at the Universität Innsbruck using a ThermoFinnigan Delta^{plus}XL. Full details are described in Spötl and Vennemann (2003). The long-term analytical uncertainty for oxygen and carbon are 0.08% and 0.06% respectively (Spötl, 2011). Each pass of the milling bit for this series removed a volume measuring 0.2 mm (along-axis: x) \times 0.5 mm (depth: z) \times 1.5 mm (across-layer: y). To reduce sampling uncertainty at this higher resolution, the position of the milling track was optimised based on the orientations of sparse visible laminae.

4. Results and discussion

4.1. Sampling interval and sampling error calculation

A total of 43 contour lines were sampled (Fig. 3b). To obtain sufficient sample mass to perform the isotopic dating (~ 15 mg), we combined every two successive ~ 250 - μm -thick samples into a composite ~ 500 - μm thick sample over the first 42 samples (i.e. 21 dating samples). Powder milled from the 43rd (youngest) contour was retained as a single ~ 250 - μm thick sample, giving a total of 22 dating samples.

To estimate the maximum likely sampling error in the ‘inaccessible’ z dimension using the x, y contour data, we assumed that the geometry of crystal terminations (and thus growth horizons) visible in the x, y plane is representative of the crystal termination geometry expected in the x, z plane (Fig. 4). Based on all of the contour data, the maximum x displacement (Δx_{max}) for all possible 0.8 mm increments of y (i.e. $\Delta y = 0.8$ mm, the equivalent of the milling depth) was calculated to be 0.34 mm (Fig. 4). We assume this to be a reliable proxy for the maximum displacement of z in the x – z plane (i.e. Δz) based on a 0.8 mm milling depth. Using trigonometric relationships, 0.34 mm corresponds to an angle of $\sim 23^\circ$ from the vertical at a depth of 0.8 mm, from which we calculate the equivalent along-growth-axis distance (i.e. perpendicular to the growth layers) as 0.31 mm. As shown in Fig. 4, this represents an estimate of the potential maximum thickness of stratigraphically younger calcite (or stratigraphically older calcite if the lamination pattern is orientated in the opposite direction) erroneously sampled beyond the nominal, or intended, sample thickness (~ 0.5 -mm). As a precaution, we have rounded this up to 0.40 mm in case the geometry we observe in the x, y plane underestimates the true geometry in the x, z plane. Given that we do not know if the Δz is ‘positive’ (incorporating older material) or ‘negative’ (incorporating younger material) with respect to the x -axis of CD3 growth, the 0.4 mm uncertainty applies in both directions (i.e. ± 0.4 mm). For a given sample, therefore, the assigned stratigraphic position is taken as the midpoint of the layer in mm (determined using its average depth below the previous layer), and the maximum stratigraphic thickness of each sample is taken to lie within plus or minus the sum of 0.4 mm and half of the average nominal sample layer thickness. For example, for a sample with a nominal layer thickness of 0.55 mm and a midpoint situated at 12.5 mm from the top of the section, the relative depth position and maximum stratigraphic width above and below this point is expressed as

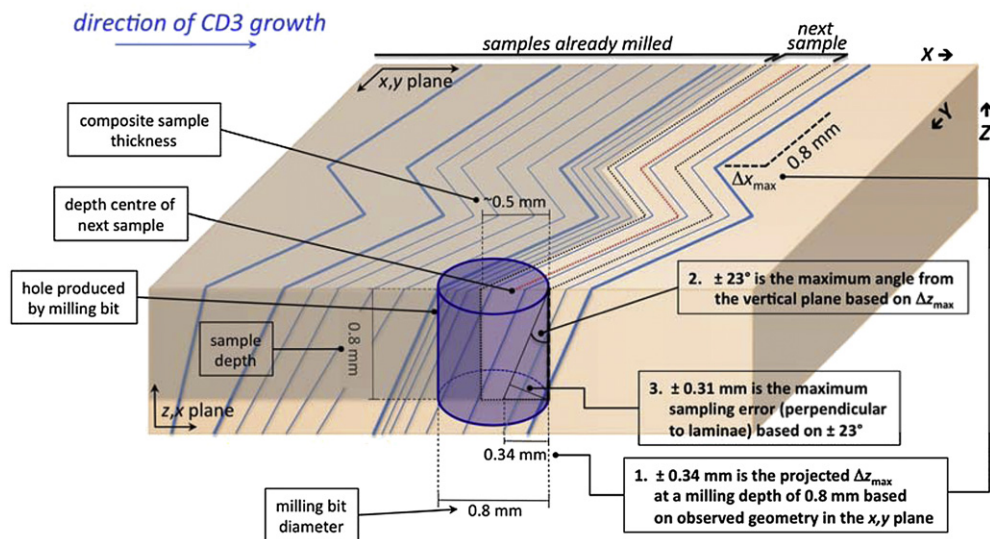


Fig. 4. Idealised view of the geometry of CD3 growth layering and the calculation of sampling error. Blue zig-zag lines are the growth layers. The grey shaded region represents the already-milled section, whilst the black dotted lines delineate the next composite sample to be milled based on the current position of the milling bit (indicated by the cylindrical bore hole). The red dotted line is the centreline of this next sample. The maximum x displacement (Δx_{\max}) per equivalent milling depth (0.8 mm) calculated from the lamination geometry observed in the x, y plane is used as a proxy for Δz_{\max} , which is a geometric estimate of unintentionally sampled material due to the unknown lamination pattern in the x, z plane. Based on a maximum angle from the vertical of 23° , this produces a maximum deviation from the nominal milling position of ± 0.31 mm. (For interpretation of the references to colour in this figure legend, the reader is referred to the web version of this article.)

12.5 ± 0.675 mm, i.e. $\pm (0.4 + [0.55/2])$ mm). In other words, the maximum stratigraphic envelope for this sample extends from 11.825 to 13.175 mm. We stress that this is a conservative estimate (i.e. an overestimate) of true sampling uncertainty, especially given that the designated error in the z dimension (0.4 mm) exceeds the maximum value derived from all available contour data (0.34 mm), as stated above. For each sample, this calculated depth range was propagated into the final age model to generate age-model age uncertainties over the entire analysed section.

A potential additional source of sampling error is the effect of the ‘wash-out time’ relative to the laser scan speed. The aerosol plume from a given laser spot position reaches the mass spectrometer some time (the wash-out time) after the laser has passed the sampling point. The time-resolved mass spectrometry data are thus out of phase with the time-resolved laser position by the product of the laser scan speed and the wash-out time. The sampling uncertainty arising from this phenomenon thus increases as both wash-out time and scan speed increase. The order-of-magnitude wash-out time for our LA-ICP-MS system is ~ 1 s. Based on a scan speed of $100 \mu\text{m s}^{-1}$, this equates to a sampling position/mass spectrometry offset equivalent to 103 μm , which implies an average age uncertainty of ~ 330 yr. However, the range of elemental variations observed in the CD3 section studied here represents a maximum of \sim one-third of an order of magnitude (Fig. 3), which would reduce this effect down to around 30 μm , equivalent to ~ 100 yr. We regard this potential source of sampling error as negligible given the magnitude of the sampling uncertainties arising from the micromilling.

4.2. Uranium–thorium age results

The results of the uranium and thorium isotopic measurements are shown in Table 2. As with previous Corchia Cave speleothems, CD3 contains relatively low amounts of common thorium as indicated by the measured ($^{230}\text{Th}/^{232}\text{Th}$) activities (Table 1). However, the CD3 values are lower by about a factor of three than those measured from Corchia stalagmites (Drysdale et al., 2004, 2005,

2007, 2009; Zanchetta et al., 2007). We suspect this is due to the greater likelihood of detrital material being captured in a large pool compared with stalagmite drip waters. Correction for an initial ($^{230}\text{Th}/^{232}\text{Th}$) activity of 1.5 ± 1.5 yielded age adjustments of $\leq +0.5\%$ relative to the uncorrected age. The U concentrations in CD3 are also lower (by up to a factor of ~ 10) than those of stalagmites from the same chamber (e.g. Drysdale et al., 2005) in spite of their relatively similar source water concentrations (pool water: 6.7 ± 1.2 ppb [$n = 11$], drip site CNR2: 4.2 ppb ± 0.7 ppb [$n = 13$], unpublished data; for further drip and pool saple information, see Baneschi et al. (2011)). This suggests a smaller U partitioning coefficient for the subaqueous calcite compared to the stalagmite calcite.

All corrected ages are in stratigraphic order within 2σ age uncertainties, as portrayed in the depth–age plot (Fig. 5a). The 2σ age uncertainty averages 6.4 ka, and ranges between 3.9 ka (CD3-226; 1.7% precision) and 8.7 ka (CD3-216; 3.2% precision) (Table 1). Given the homogeneity of the samples, the magnitude of U–Th age uncertainty cannot be attributed to inadvertent sample cross contamination due to the contour interpolation procedure. The large negative and positive errors at the youngest and oldest ends of the depth–age model (respectively) reflect the time-unanchored extremities of the section. The age-versus-age-uncertainty plot derived from the depth–age modelling (Fig. 5b) portrays a continuous series of age uncertainty through time, and thus provides interpolated age and 2σ age error constraints for any depth position along the profile (except at the extremes for the reasons stated above). As this series shows, some intervals of the profile display uncertainties greater than those evident in the corrected U-series ages. Ignoring the inflated values at the extremities, the mean model age error is 4.8 ka but the maximum model error is 11.4 ka. Again, the magnitude of the error cannot be related to the sampling technique. Instead, model error is strongly influenced by age density, i.e. the number of ages per unit time (and not per unit depth). This is clearly seen in Fig. 6.

In summary, there is convincing evidence that the magnitude of both U-series age errors and model-age errors can be attributed to

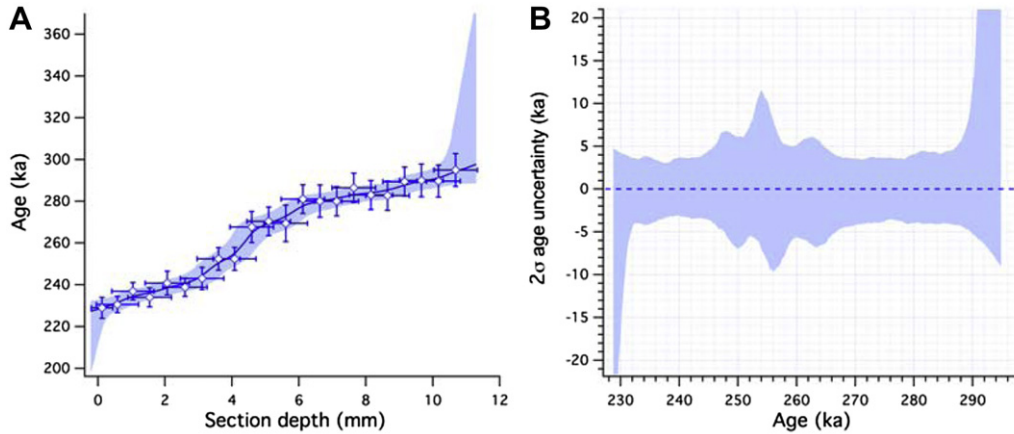


Fig. 5. (a) Depth–age plot for CD3. Horizontal error bars are \pm maximum sample depth uncertainties and vertical errors bars are the $\pm 2\sigma$ U-series age errors. (b) Age uncertainty ($\pm 2\sigma$) versus age derived from the Monte-Carlo depth–age modelling.

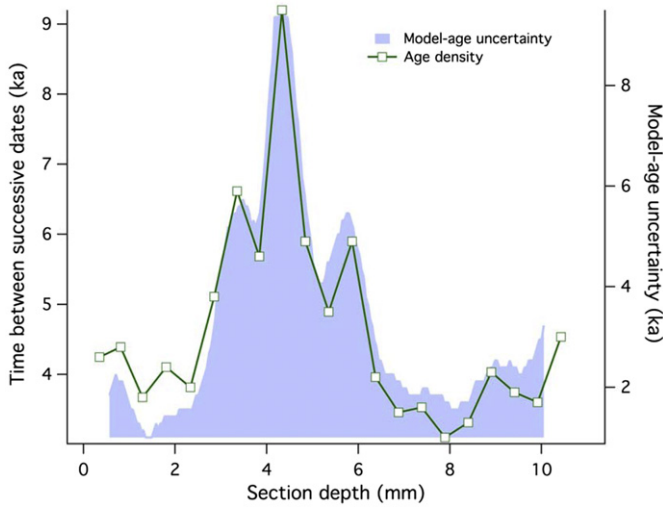


Fig. 6. Comparison between age density (i.e. the age difference between each successive pair of age-model ages for the corresponding U-series sampling depths) and the model-age errors (calculated as the average of the $+2\sigma$ and -2σ errors for each interpolated age data point) versus depth along the CD3 section.

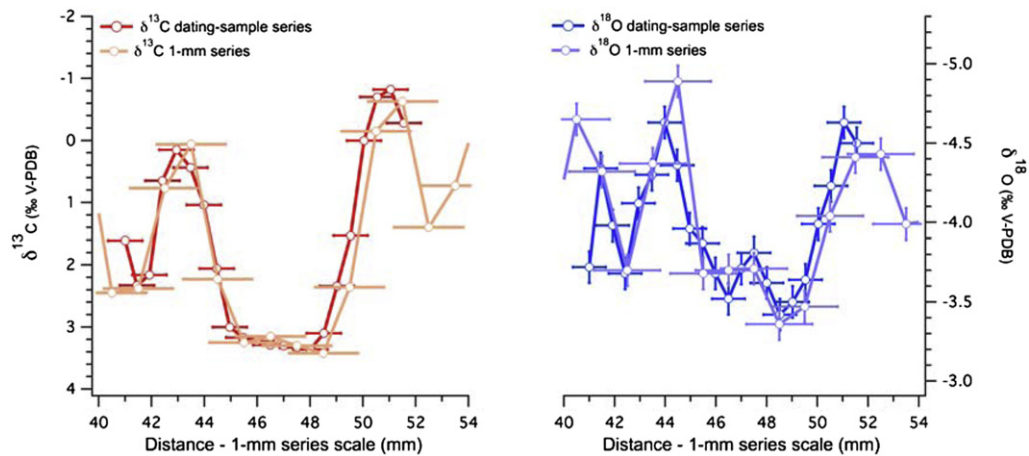


Fig. 7. Comparison between the CD3 stable isotope profiles (C: red; O: blue) from the section under investigation in this study and corresponding segment of a previously analysed 1-mm series spanning the same time period (C: pink; O: violet). The vertical error bars (hidden by the symbols for carbon) are the analytical uncertainties (1σ) of the isotope analyses and the horizontal error bars are the spatial uncertainties in the drilling (1-mm series) or milling (dating-sample series – this study). The distance scale for the dating samples has been adjusted by a constant (+40.88 mm) to align it with the depth scale of the 1-mm series. (For interpretation of the references to colour in this figure legend, the reader is referred to the web version of this article.)

entirely plausible causes that are unrelated to the contour-based sampling method described here.

4.3. Comparisons with stable isotope data

A more robust test of the reliability of our technique is to compare the dating-sample isotopic profile from this study with profiles previously derived from conventional drilling. Gross sampling errors due to the incorrect interpolation of the contours should result in a significant loss of resolution (i.e. smoothing) in the stable isotope profile of the dating samples. The 1 mm series with which we compare our new data was drilled to a depth of 2 mm, so based on the observations on the experimental section from this study and the relationships shown in Fig. 4, we can assign a maximum spatial uncertainty of ± 1.3 mm from the central point of each 1 mm sample (i.e. ± 0.5 mm of drill radius and a maximum ± 0.8 mm of calcite due to the uncertainty in the x, z plane). Fig. 7 shows that the two isotope profiles compare favourably.

Comparison between the dating-sample isotope series and the much-better-resolved 200- μm isotope series from the Innsbruck laboratory yields a similarly favourable result (Fig. 8). The sampling uncertainty on the 200- μm series is much lower due to the smaller

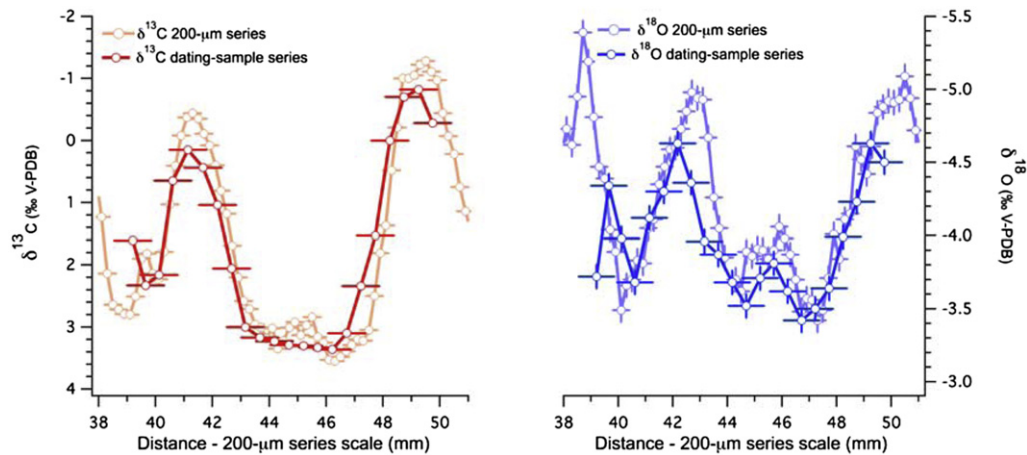


Fig. 8. Comparison between the CD3 stable isotope profiles (C: red; O: blue) from the section under investigation in this study and the corresponding segment of a previously analysed 200- μm series spanning the same time period (C: pink; O: violet). The vertical and horizontal error bars are as per Fig. 7. The distance scale for the dating samples has been adjusted by a constant (+39.08 mm) to align it with the depth scale the scale of the 200- μm series. (For interpretation of the references to colour in this figure legend, the reader is referred to the web version of this article.)

sampling depth and the practice of following a track extending perpendicular to the growth layers; we estimate this uncertainty to be no more than $\pm 300 \mu\text{m}$ from the centre point of each sample. Consequently, the isotopic resolution of the Innsbruck series is considerably higher than that of the dating-sample series (Fig. 8). Given that a small degree (i.e. a few tenths of a per mille) of isotopic variation should be expected across any growth horizon, and bearing in mind the laterally variable lamina thickness of the dated section (Figs. 2 and 3) and the different sampling resolutions and uncertainties associated with the other two profiles, the high degree of replication of the two isotope profiles suggests gross sampling errors have not been introduced during our contouring procedure.

5. Conclusions

Speleothems that lack visible layering are difficult to sample for stable-isotopic dating at high-spatial resolution. To overcome this, we have applied a new method to a section of a subaqueous speleothem based on the micromilling of contours derived from 2D trace-element imaging. The relatively consistent distribution of the trace elements Mg, Sr and Ba along individual time horizons in this speleothem allows distinctive growth layers to be resolved. By digitising the most prominent of these layers as contours, then interpolating over the studied section, we were able to generate 22 samples for U-series dating spaced at $\sim 500 \mu\text{m}$ increments.

The MC-ICP-MS analyses of these samples returned ages in correct stratigraphic sequence within 2σ dating errors. The magnitude of the raw age uncertainties as well as age-model age uncertainties were found to be unlikely related to the sampling procedure but instead most likely due to analytical error and the number of age density respectively. Comparison of stable isotope profiles from the dating samples and two other isotope series from the same time interval in CD3 revealed good agreement between the individual series.

The method we describe is applicable to any speleothem lacking regular visible growth layering, as long as across-layer consistency of trace element concentrations can be demonstrated. Although the use of conventional sampling methods would be reasonable where such speleothems are sufficiently old (such that analytical errors will have more influence than sampling error) and have grown fast enough to counter the problems of sampling error, we suggest our method is particularly useful where high spatial precision is

required, as is the case with slow-growing and/or very young speleothem calcite. Reduction of sampling errors could be achieved by extending the width of the imaged region (and thus the contoured area), which would allow the investigator to reduce sampling depth, the greatest source of sampling error.

Acknowledgements

This work was funded by the Australian Research Council 'Discovery Projects' scheme (DP110102185). We thank Siro Moggio for assistance with the IRMS analyses. Recovery of the CD3 core would not have been possible without the logistical support of the Federazione Speleologica Toscana and the Gruppo Speleologico Lucchese. We are grateful for reviewers Dr Wolfgang Müller and Dr Leonid Neymark whose comments significantly improved the manuscript.

Editorial handling by: D. Richards

References

- Baneschi, I., Piccini, L., Regattieri, E., Isola, I., Guidi, M., Lotti, L., Mantelli, F., Menichetti, M., Drysdale, R.N., Zanchetta, G., 2011. Hypogean microclimatology and hydrology of the 800–900 m asl level in the Monte Corchia cave (Tuscany, Italy): preliminary considerations and implications for paleoclimatological studies. *Acta Carsologica* 40, 175–187.
- Cheng, H., Edwards, R.L., Hoff, J., Gallup, C.D., Richards, D.A., Asmerom, Y., 2000. The half-lives of uranium-234 and thorium-230. *Chemical Geology* 169, 17–33.
- Coplen, T.B., Winograd, I.J., Landwehr, J.M., Riggs, A.C., 1994. 500,000-year stable carbon isotopic record from Devils Hole, Nevada. *Science* 263, 361–365.
- Couchoud, I., Drysdale, R.N., Hellstrom, J.C., Zanchetta, G., Regattieri, E., Isola, I., 2011. A precisely dated speleothem record of Termination III and marine isotope stage 7 from Corchia cave, Italy. In: *Climate Change: the Karst Record*, 6th International Conference, p. 33. Abstract book.
- Drysdale, R.N., Zanchetta, G., Hellstrom, J.C., Fallick, A.E., Zhao, J.X., Isola, I., Bruschi, G., 2004. Palaeoclimatic implications of the growth history and stable isotope ($\delta^{18}\text{O}$ and $\delta^{13}\text{C}$) geochemistry of a Middle to Late Pleistocene stalagmite from central-western Italy. *Earth and Planetary Science Letters* 227, 215–229.
- Drysdale, R.N., Zanchetta, G., Hellstrom, J.C., Fallick, A.E., Zhao, J.X., 2005. Stalagmite evidence for the onset of the Last Interglacial in southern Europe at 129 ± 1 ka. *Geophysical Research Letters* 32, L24708. <http://dx.doi.org/10.1029/2005GL024658>.
- Drysdale, R.N., Zanchetta, G., Hellstrom, J.C., Fallick, A.E., McDonald, J., Cartwright, I., 2007. Stalagmite evidence for the precise timing of North Atlantic cold events during the early last glacial. *Geology* 35, 77–80.
- Drysdale, R.N., Hellstrom, J.C., Zanchetta, G., Fallick, A.E., Sánchez Goñi, M.F., Couchoud, I., McDonald, J., Maas, R., Lohmann, G., Isola, I., 2009. Evidence for obliquity forcing of glacial termination II. *Science* 325, 1527–1531.
- Drysdale, R.N., Couchoud, I., Zanchetta, G., Hellstrom, J.C., Spötl, C., Woodhead, J.D., Perrette, Y., Baneschi, I., Bajo, P., Gagan, M.K., Isola, I., Greig, A., 2011. The last 11

- glacial-interglacial cycles recorded in a single speleothem from Corchia Cave. In: *Climate Change: The Karst Record*, 6th International Conference, p. 42. Abstract book.
- Eggins, S.M., Grün, R., McCulloch, M.T., Pike, A.W.G., Chappell, J., Kinsley, L., Mortimer, G., Shelley, M., Murray-Wallace, C.V., Spötl, C., Taylor, L., 2005. In situ U-series dating by laser-ablation multi-collector ICPMS: new prospects for Quaternary geochronology. *Quaternary Science Reviews* 24, 2523–2538.
- Fairchild, I.J., Smith, C.L., Baker, A., Fuller, L., Spötl, C., Mathey, D., McDermott, F., 2006. Modification and preservation of environmental signals in speleothems. *Earth-Science Reviews* 75, 105–153.
- Folk, R.L., Assereto, R., 1976. Comparative fabrics of length-slow and length-fast calcite and calcitized aragonite in a Holocene speleothem, Carlsbad Cavern, New Mexico. *Journal of Sedimentary Petrology* 46 (3), 486–496.
- Hellstrom, J., 2003. Rapid and accurate U/Th dating using parallel ion-counting multi-collector ICP-MS. *Journal of Analytical Atomic Spectrometry* 18, 1346–1351.
- Hellstrom, J., Paton, C., Woodhead, J., Hergt, J., 2008. Iolite: software for spatially resolved LA-(quad and MC) ICPMS analysis. *Mineralogical Association of Canada Short Course Series* 40, 343–348.
- Hendy, E., Tomiak, P., Collins, M., Hellstrom, J., Tudhope, A., Lough, J., Penkman, K., 2012. Assessing amino acid racemization variability in coral intra-crystalline protein for eochronological applications. *Geochimica et Cosmochimica Acta* 86, 338–353.
- Kolesar, P.T., Riggs, A.C., 1999. Form and formation: speleothems in Devils Hole, a tectonic cave in southern Nevada. *Geological Society of America, Abstracts with Programs* 31 (7), A-90.
- Kolesar, P.T., Riggs, A.C., 2004. Influence of depositional environment on Devil's Hole calcite morphology and petrology. In: Sasowsky, I.D., Mylroie, J. (Eds.), *Studies of Cave Sediments - Physical and Chemical Records of Paleoclimate*. Kluwer Academic/Plenum Publishers, New York, pp. 227–241.
- Martrat, B., Grimalt, J.O., Shackleton, N.J., de Abreu, L., Hutterli, M.A., Stocker, T.F., 2007. Four climate cycles of recurring deep and surface water destabilizations on the Iberian margin. *Science* 317, 502–507.
- Paton, C., Hellstrom, J., Paul, B., Woodhead, J., Hergt, J., 2011. Iolite: freeware for the visualisation and processing of mass spectrometer data. *Journal of Analytical Atomic Spectrometry* 26, 2508–2518.
- Paul, B., Paton, C., Norris, A., Woodhead, J., Hellstrom, J., Hergt, J., Greig, A., 2012. CellSpace: a module for creating spatially registered laser ablation images within the Iolite freeware environment. *Journal of Analytical Atomic Spectrometry* 27, 700–706. <http://dx.doi.org/10.1039/c2ja10383d>.
- Piccini, L., Zanchetta, G., Drysdale, R.N., Hellstrom, J., Isola, I., Fallick, A.E., Leone, G., Doveri, M., Mussi, M., Mantelli, F., Molli, G., Lotti, L., Roncioni, A., Regattieri, E., Meccheri, M., Vaselli, L., 2008. The environmental features of the Monte Corchia cave system (Apuan Alps, central Italy) and their effects on speleothem growth. *International Journal of Speleology* 37, 153–172.
- Richards, D.A., Dorale, J.A., 2003. U-series chronology of speleothems and paleoclimate. Uranium-series geochemistry. *Reviews in Mineralogy and Geochemistry* 52, 407–460.
- Scholz, D., Hoffmann, D., Hellstrom, J., Bronk Ramsay, C., 2012. A comparison of different methods for speleothem age modelling. *Quaternary Geochronology* 14, 94–104.
- Spötl, C., 2011. Long term performance of the Gasbench isotope ratio mass spectrometry system for the stable isotope analysis of carbonate microsamples. *Rapid Communications in Mass Spectrometry* 25, 1683–1685. <http://dx.doi.org/10.1002/rcm.5037>.
- Spötl, C., Vennemann, T.W., 2003. Continuous-flow IRMS analysis of carbonate minerals. *Rapid Communications in Mass Spectrometry* 17, 1004–1006.
- Spötl, C., Mathey, D., 2012. Scientific drilling of speleothems – a technical note. *International Journal of Speleology* 41 (1), 29–34.
- Winograd, I.J., Coplen, T.B., Landwehr, J.M., Riggs, A.C., Ludwig, K.R., Szabo, B.J., Kolesar, P.T., Revesz, K.M., 1992. Continuous 500,000-year climate record from vein calcite in Devils Hole, Nevada. *Science* 258, 255–260.
- Winograd, I.J., 2002. Evidence from uranium-series-dated speleothems for the timing of the penultimate deglaciation of northwestern Europe. *Quaternary Research* 58, 60–61.
- Woodhead, J., Hellstrom, J., Hergt, J.M., Greig, A., Maas, R., 2007. Isotopic and elemental imaging of geological materials by laser ablation inductively coupled plasma-mass spectrometry. *Geostandards and Geoanalytical Research* 31, 331–343.
- Zanchetta, G., Drysdale, R.N., Hellstrom, J.C., Fallick, A.E., Isola, I., Gagan, M.K., Pareschi, M.T., 2007. Enhanced rainfall in the Western Mediterranean during deposition of sapropel S1: stalagmite evidence from Corchia cave (Central Italy). *Quaternary Science Reviews* 26, 279–286.